The Journal of Experimental Biology 209, 731-747
Published by The Company of Biologists 2006
doi:10.1242/jeb.02032

A potassium channel (Kv4) cloned from the heart of the tunicate *Ciona intestinalis* and its modulation by a KChIP subunit

Vicenta Salvador-Recatalà[1,2], Warren J. Gallin[3], Jennifer Abbruzzese[4], Peter C. Ruben[4] and Andrew N. Spencer[2,3,*]

[1]*Department of Physiology, University of Alberta, Edmonton, AB, T6G 2H7, Canada,* [2]*Bamfield Marine Sciences Centre, Bamfield, BC, V0R 1B0, Canada,* [3]*Department of Biological Sciences, University of Alberta, Edmonton, AB, T6G 2E9, Canada, and* [4]*Department of Biology, Utah State University, Utah, 84322 USA*

*Author for correspondence (e-mail: andy.spencer@shaw.ca)

Accepted 10 December 2005

Summary

Voltage-gated ion channels of the Kv4 subfamily produce A-type currents whose properties are tuned by accessory subunits termed KChIPs, which are a family of Ca^{2+} sensor proteins. By modifying expression levels and the intrinsic biophysical properties of Kv4 channels, KChIPs modulate the excitability properties of neurons and myocytes. We studied how a Kv4 channel from a tunicate, the first branching clade of the chordates, is modulated by endogenous KChIP subunits. BLAST searches in the genome of *Ciona intestinalis* identified a single *Kv4* gene and a single *KChIP* gene, implying that the diversification of both genes occurred during early vertebrate evolution, since the corresponding mammalian gene families are formed by several paralogues. In this study we describe the cloning and characterization of a tunicate Kv4 channel, *Ciona*Kv4, and a tunicate KChIP subunit, *Ciona*KChIP. We demonstrate that *Ciona*KChIP strongly modulates *Ciona*Kv4 by producing larger currents that inactivate more slowly than in the absence of the KChIP subunit. Furthermore, *Ciona*KChIP shifted the midpoints of activation and inactivation and slowed deactivation and recovery from inactivation of *Ciona*Kv4. Modulation by *Ciona*KChIP requires the presence of the intact N terminus of *Ciona*Kv4 because, except for a minor effect on inactivation, *Ciona*KChIP did not modulate *Ciona*Kv4 channels that lacked amino acids 2–32. In summary, our results suggest that modulation of Kv4 channels by KChIP subunits is an ancient mechanism for modulating electrical excitability.

Key words: Kv4, KChIP, potassium channel, *Ciona intestinalis*, tunicate, heart.

Introduction

Voltage-gated potassium channels related to *Drosophila Shal* are encoded in mammals by the *Kv4* gene subfamily (Kv4.1: Pak et al., 1991; Kv4.2: Roberds and Tamkun, 1991; and Kv4.3: Serôdio et al., 1994). Kv4 channels mediate transient outward currents in cardiac myocytes (Dixon et al., 1996), smooth muscle (Amberg et al., 2002) and neurons (Serôdio et al., 1994). The currents mediated by Kv4 channels play important roles in specifying the firing properties of molluscan and lobster neurons (Connor and Stevens, 1971; Baro et al., 1996), suggesting that Kv4 channels are conserved determinants of cellular excitability. The three mammalian Kv4 channel isoforms differ in their biophysical properties. For example, the fast component of inactivation of Kv4.1 channels contributes significantly less to inactivation than the fast inactivating component of Kv4.2 and Kv4.3 channels (Pak et al., 1991; Jerng and Covarrubias, 1997). The full significance of these differences in properties between the three Kv4 channel isoforms is not yet understood. However, since expression of Kv4.2 and Kv4.3 isoforms is complementary in brain and heart (Serôdio et al., 1996), it seems likely that the specific properties of each of these isoforms contribute to determining the function of the particular tissue area where it is expressed. These differences between the three Kv4 channel isoforms likely represent adaptive features of these channels. To identify adaptive and conserved features of mammalian Kv4 channels it is necessary to compare these with invertebrate Kv4 channels such as jellyfish *Shal* (Jegla and Salkoff, 1997), arthropod *Shal* (Baro et al., 1996) and a tunicate *Shal* (Nakajo et al., 2003).

KChIPs, a family of Ca^{2+} binding proteins (Burgoyne and Weiss, 2001), are integral components of Kv4 channel supramolecular complexes (An et al., 2000). KChIP isoforms 1–3, but not KChIP4, increase the density of Kv4 currents (Shibata et al., 2003). All four KChIP isoforms modify the kinetics and gating properties of Kv4 channels (An et al., 2000; Holmqvist et al., 2002). Modulation of Kv4 channels by KChIP subunits is likely a conserved mechanism to modulate tissue

excitability, because the effects of human KChIP1 on the lobster and mammalian Kv4 channels are similar (Zhang et al., 2003). Thus, KChIP1 increased current amplitude, slowed the rate of inactivation, and shifted activation and inactivation midpoints of lobster Kv4 channels (Zhang et al., 2003). In the present study, we address the question of how tunicate Shal is modulated by endogenous KChIP subunits.

The vertebrate multi-gene *Kv4* and *KChIP* families are represented by single genes in the tunicate genome. Scaffolds 168 and 457 of the genome database for *Ciona intestinalis* (http://genome.jgi-psf.org/ciona4/ciona4.home.html, release version 1.0) contain the *Kv4* and the *KChIP* gene, respectively. We cloned the transcripts for a Kv4 channel (*Ciona*Kv4) and a KChIP subunit (*Ciona*KChIP) from myocardial tissue of *Ciona intestinalis*. Repolarization of the action potential in the tunicate heart is complex with several repolarization phases, which are presumably an adaptation for pumping blood by means of peristaltic contractions that can propagate in both directions through the tubular heart (Kriebel, 1967). Since Kv4 channels play a crucial role in determining the excitability properties of cardiac tissues of vertebrates, we suspected that these channels were playing a similar role in the tunicate heart.

We characterized the potassium currents produced by *Ciona*Kv4 channels heterologously expressed in *Xenopus* oocytes, in the presence and absence of *Ciona*KChIP. Our biophysical data for *Ciona*Kv4 reinforces and complements what is known for tunicate *Shal* (Nakajo et al., 2003). Because the N terminus of Kv4 channels appears to be essential for modulation by KChIP (Bähring et al., 2001b), an N-terminal deletion mutant of *Ciona*Kv4, lacking amino acids 2–32, was constructed (nt*Ciona*Kv4), and the effects of *Ciona*KChIP on this mutant *Ciona*Kv4 channel were evaluated. In this paper we describe the modulation of kinetic and gating parameters of a tunicate Shal channel (*Ciona*Kv4) by a tunicate KChIP subunit (*Ciona*KChIP), the first KChIP subunit cloned from either an invertebrate or a non-vertebrate chordate. Our data and those provided by Zhang et al. (2003) on modulation of lobster Shal by KChIP1, are the first indications that modulation of Kv4 channels by KChIP subunits might be an ancient mechanism to modulate the excitability of electrically active tissues.

Materials and methods

Tissue and RNA extraction

Specimens of *Ciona intestinalis* (Linnaeus 1767) were purchased from the Marine Biology Laboratory (Woods Hole, MA, USA) and kept in a seawater aquarium at 12°C until used. The heart, enclosed in the pericardium, was excised in diethyl pyrocarbonate (DEPC)-treated artificial seawater whose composition was (in mmol l^{-1}): NaCl (425), KCl (9), $CaCl_2$ (9.3), $MgSO_4$ (25.5), $MgCl_2$ (23), Hepes (10). This heart complex was pinned onto a base of Sylgard (Dow Corning, Midland, MI, USA) in a Petri dish and the pericardium and raphe (connective tissue that joins the pericardium to the myocardium) were cut away. The isolated myocardium was rinsed in filtered DEPC-treated artificial seawater several times in order to remove any remaining blood cells and cellular debris and then frozen at –80°C. Total RNA was extracted from heart tissue (4–6 hearts per experiment) using the 'Totally RNA' kit (Ambion, Austin, TX, USA).

Rapid amplification of cDNA 3′ end (3′-RACE) for Kv4 and KChIP homologues

The GeneRacer Kit (Invitrogen, Carlsbad, CA, USA) was used to perform a 3′-RACE assay. Briefly, cDNA was synthesized from total RNA using an oligo-dT primer, with a unique sequence at the 3′ end, provided with the kit. Each 50 μl 3′-RACE assay contained: 1× Opti-Prime Buffer (Stratagene, La Jolla, CA, USA) (10 mmol l^{-1} Tris-HCl, 1.5 mmol l^{-1} $MgCl_2$, 25 mmol l^{-1} KCl, pH 8.3), 0.5 unit of Taq polymerase, 0.25 mmol l^{-1} of each dNTP, 1 μmol l^{-1} each of forward primer and reverse primer and 2 μl cDNA. The sense primers (5′-GACGGATCTACAGCCAAAATCAAAGACA-3′ for Kv4 and 5′-CAGTTGTTGGGATCGCATGT-3′ for KChIP) were bound to an internal sequence of the *Kv* channel or the *KChIP* subunit transcript; the anti-sense primer, supplied with the kit, bound to the specific sequence of the oligo-dT primer. The temperature conditions were: 30 s at 94°C, followed by 5× (30 s at 94°C, 30 s at 65°C, 3 min at 72°C), 25× (30 s at 94°C, 30 s at 60°C, 3 min at 72°C) followed by 5 min at 72°C. 3′-RACE products were sequenced with the forward primers used in these assays. Next, new forward primers were designed to bind downstream within these sequences in nested 3′-RACE assays. Successive nested RACE assays were done until the first 3′-RACE assay product was fully sequenced.

Cloning of full-length cDNA of CionaKv4 and CionaKChIP

The full-length open reading frames for *Ciona*Kv4 and *Ciona*KChIP were amplified with sense primers containing the start codon and a Kozak consensus site for the 5′ end, and anti-sense primers designed to bind downstream of the translational termination codon (*Ciona*Kv4-sense: 5′-GGCTCGAGGCCGCCACCATGGCAACAGCAGTAGC-3′; *Ciona*Kv4-antisense: 5′-GGCCTAGGCAAAGTCCCGCCGC-TACAGTGAG-3′; *Ciona*KChIP-sense: 5′-GGCTCGAGGCC-GCCACCATGTCTCTCGCTATCTTAACCATGGTGAC-3′; *Ciona*KChIP-antisense: 5′-GGACTAGTAACGCCAGAAA-CGCCGCCTTGATGGAGCTATAACGC-3′). Primers also contained restriction sites to allow directional insertion of the PCR products into pXT7 (Dominguez et al., 1995). Each 50 μl PCR reaction contained: 1× Opti-Prime Buffer (Stratagene, La Jolla, CA, USA; 10 mmol l^{-1} Tris-HCl, 1.5 mmol l^{-1} $MgCl_2$, 25 mmol l^{-1} KCl, pH 8.3), 0.5 unit of Taq polymerase, 1 unit of Pfu, 0.2 mmol l^{-1} of each dNTP, 1 μmol l^{-1} each of forward primer and reverse primer, and 2 μl cDNA. Temperature conditions were: 30 s at 94°C, 25× (30 s at 94°C, 30 s at 60°C, 3 min at 72°C) followed by 5 min at 72°C. The resulting PCR products were then digested with appropriate restriction enzymes, ligated with appropriately digested pXT7 plasmid

and transformed into *E. coli.* Clones were sequenced to verify that no mutation had been introduced by PCR. This construct was linearized with *Sal*I and cRNA was synthesized using the T7 mMessage mMachine kit (Ambion, Austin, TX, USA).

Construction of the N-truncation mutant (ntCionaKv4) of CionaKv4

To generate a mutant channel lacking amino acids 2–32 of the N terminus domain, a diluted sample of the *Ciona*Kv4 clone was amplified by PCR. The composition of the PCR reactions and the temperature conditions were as described in the previous section. The forward primer (5′-GGCTCGAG-GCCGCCACCATGAACCGACGTAAAACAAAAGAC-3′) was designed to bind to the *Ciona*Kv4 clone, starting from nucleotide 97. A start codon, Kozak consensus sequence and an *Xho*I site were added to this sequence. The reverse primer was the same as used for the full-length clone. These PCR products were inserted into pXT7 and transformed into *E. coli*. Clones were sequenced to verify the deletion and to check that the undeleted sequence had no mutations introduced by PCR.

Alignment and phylogenetic tree

Amino acid sequences of a set of phylogenetically representative Kv4 channels (18) and KChIP subunits (17) were aligned with T-Coffee software (Notredame et al., 2000). Kv4 channel regions that contained extensive gaps were edited out, leaving a data matrix that included the T1 domain and the membrane-spanning core (trans-membrane domains S1 to S6), giving a total of 405 characters. MrBayes v3.0b (Huelsenbeck and Ronquist, 2001) was used to determine the phylogenetic relationships of the channel sequences. The default parameters for protein sequences were used. A total of 200 000 cycles were run; the topology and branch length of every 100th tree was saved. The Bayesian maximum likelihood tree was obtained by taking a consensus of the collected trees after a 101 tree burn-in. The nodes on the tree are labelled with the posterior probability for each node; nodes with a probability of one were left unlabelled. The tree was visualized using Treeview (Page, 1996).

Oocyte preparation

Oocytes from *Xenopus laevis* were surgically removed and dissociated using 2 mg ml^{-1} collagenase 1A (Sigma Aldrich, St Louis, MO, USA) in a solution containing (in mmol l^{-1}): NaCl (96), KCl (4), $MgCl_2$ (20) and Hepes (5), pH 7.4. Oocytes were incubated at 18°C in culture medium containing (in mmol l^{-1}): NaCl (96), KCl (2), $MgCl_2$ (1), $CaCl_2$ (1.8), Hepes (5), sodium pyruvate (2.5), pH 7.4 with 100 mg l^{-1} gentamycin and 3% horse serum (Gibco BRL, Carlsbad, CA, USA). 24 or 48 h following oocyte isolation, 40 nl of *Ciona*Kv4 cRNA (~16 ng) or nt*Ciona*Kv4 (~8 ng) were injected into each *Xenopus* oocyte. For co-expression experiments, 20 nl (~8 ng) of *Ciona*Kv4 or 20 nl (~4 ng) of nt*Ciona*Kv4 cRNA solution was mixed with 20 nl (~7 ng) of *Ciona*KChIP cRNA solution, to give a final volume of 40 nl that was injected into each oocyte. The approximate molar ratio was [1 *Ciona*Kv4:3 *Ciona*KChIP] or [1 nt*Ciona*Kv4:6 *Ciona*KChIP]. Immediately prior to each experiment the vitelline membrane was manually removed with forceps after treatment in a hyperosmotic solution containing (in mmol l^{-1}): NaCl (96), KCl_2 (2), $MgCl_2$ (20), Hepes (5) and mannitol (400), pH 7.4.

Voltage-clamp recordings

All recordings were made from cell-attached macro-patches. The pipettes contained ND96 solution, with the following composition (in mmol l^{-1}): NaCl (96), KCl (2), $MgCl_2$ (1), $CaCl_2$ (1.8) and Hepes (5), pH 7.4. During the recordings, oocytes were bathed in a grounded, isopotential solution, thereby ensuring that the potential applied by the recording pipette would be the true membrane potential for the macro-patch. This bath solution contained (in mmol l^{-1}): NaCl (9.6), KCl (88), EGTA (11), Hepes (5), pH 7.4. Patch pipettes were pulled from aluminosilicate glass, coated with dental wax, and fire-polished before each experiment. Only pipettes that had resistances between 0.7 and 1.4 MΩ were used.

Membrane seals were obtained by applying negative pressure. Voltage-clamp and data acquisition were carried out using an EPC-9 patch-clamp amplifier (HEKA, Lambrecht, Germany) controlled with PULSE software (HEKA) running on a Power MacIntosh G4 computer. Data were acquired at sampling intervals of 50 μs and low-pass filtered at 5 kHz during acquisition. Bath temperature was maintained at 12±0.2°C using a Peltier device controlled by an HCC-100A temperature controller (Dagan, Minneapolis, MN, USA). The holding potential was set at –100 mV and leak subtraction was performed with a P/4 protocol. PulseFit (HEKA), Igor Pro (Wavemetrics, Lake Oswego, OR, USA) and Instat (GraphPad Software, San Diego, CA, USA) software were used for analyses and graphing.

Conductances were calculated using the equation $G_K=I_{peak}/(V-E_K)$, where G_K is the potassium conductance, I_{peak} is the peak measured amplitude of the K^+ current to a test pulse, V is the voltage at which the current was measured, and E_K is the measured potassium equilibrium potential, in this case –90 mV. Conductance–voltage relationships and steady-state inactivation curves were fitted in Igor Pro by a sigmoid (Boltzmann) distribution of the form: $f(V)=G_{max}/\{1+\exp[(V_{0.5}-V)/K]\}$, where G_{max} is the maximal conductance, V is the voltage of the depolarizing pulse (for activation) or the prepulse voltage (for inactivation), and K is the slope factor. For a first order Boltzmann, used to fit conductance–voltage relationships and steady-state inactivation curves, $V_{0.5}$ is the voltage at which activation or inactivation is half maximal.

Time constants of activation were obtained from a fit of the rising phase of the currents to the Hodgkin–Huxley model of the form: $I(t)=I_{max}[1-\exp(-t/\tau)]^n$ where I_{max} is the maximum current obtained in the absence of inactivation, τ is the activation time constant, t is time and n=4. To study the decay of the current as a function of time, the decaying phases of the outward currents evoked by test pulses between +30 mV and +80 mV were fitted to the equation: $I(t)=I_0+I_1\exp(-t/\tau_1)+I_2\exp(-t/\tau_2)$, where τ_1 and

τ_2 represent the fast and the slow time constants of inactivation, respectively, I_1 and I_2 represent the relative contribution of each component to inactivation, and I_0 is the offset.

To investigate the voltage dependence of the kinetics of channel closing, tail currents were evoked at several membrane potentials, from –160 to –40 mV, from a brief (10–15 ms) depolarizing pulse to +50 mV. Tail currents obtained with pulses from –160 to –100 mV were used for analyses.

The voltage dependence of steady-state inactivation was determined by measuring the peak current evoked with a depolarizing pulse to +50 mV as a function of the voltage of a preceding 10 s prepulse test (between –130 and –30 mV). A double-pulse protocol was used to assess the rate of recovery from inactivation at –100 mV. A test pulse to +50 mV of 1 s duration was separated by a recovery period (at –100 mV) of increasing duration (50–2000 ms) from a second test pulse to +50 mV. The currents evoked by the second pulse of a double-pulse protocol were normalized to the currents produced by the first pulse and plotted against the duration of the interpulse interval.

Statistical analyses

Statistical comparisons were carried out using the Student *t*-test, or the alternative Welch *t*-test when there were significant differences between the standard deviations of the two groups. Data are presented as the mean ± s.e.m., and *N* is the number of macro-patches or oocytes, because recordings from one macro-patch per oocyte were included in the analyses.

Results

Genomic structure and amino acid sequence analyses of CionaKv4 and CionaKChIP

The nucleotide sequences (ORF and 3′-untranslated region) of *Ciona*Kv4 and *Ciona*KChIP are deposited in GenBank (Accession numbers: AY514487 for *Ciona*Kv4 and AY514488 for *Ciona*KChIP). The 3′-RACE assays allowed identification of the stop codon for *Ciona*Kv4 and verification of the position of the stop codon for *Ciona*KChIP (Fig. 1A,C). This sequence information was used to design reverse primers to amplify the full ORF for both transcripts. The exon/intron organization of the genes encoding *Ciona*Kv4 and *Ciona*KChIP were deduced by comparing their cDNA sequences with the sequences of scaffolds 168 and 457 (*Ciona intestinalis* genomic database, release version 1.0), which contained the *Ciona*Kv4 and the *Ciona*KChIP gene, respectively (Fig. 1B,D). The exon sequences in the genomic database and the corresponding regions of the transcript were 96% identical for both *Ciona*Kv4

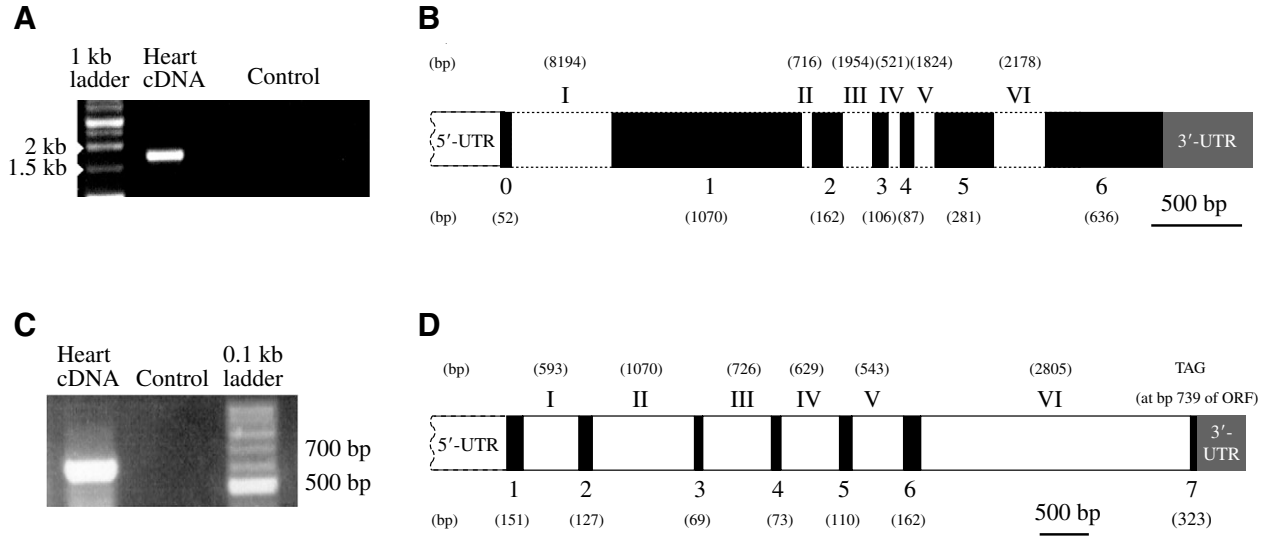

Fig. 1. RT-PCR amplification of the 3′ ends of mRNAs that encode Kv4 and KChIP, extracted from heart tissue of *C. intestinalis*. (A) Fragments of ~1500 bp corresponding to the 3′ end of the transcript for a Kv4 channel, amplified by 3′-RACE. No cDNA was added to the control reaction. (B) Diagram showing the organization of the *Ciona*Kv4 gene, based on an alignment between the transcript sequence for *Ciona*Kv4 and scaffold 168 of the genomic database for *C. intestinalis* (release version 1.0). Exons are shown as black boxes and numbered in Arabic numerals (0–6). Introns are shown as white boxes and numbered in Roman numerals (I–VI). Approximate intron sizes (in bp) are indicated above the introns. Exon sizes (in bp) are indicated below the boxes. Exon sizes, but not intron sizes, are drawn approximately to scale. The 3′-UTR region is represented by a box shaded in grey. The box representing the 5′-UTR region is delimited by a discontinuous line to indicate that the sequence of this region was not determined in the present study. (C) Fragments of ~600 bp, corresponding to the 3′ end of the transcript for a KChIP subunit, amplified by 3′-RACE. No cDNA was added to the control reaction. (D) Diagram showing the exon/intron structure of the *Ciona*KChIP gene, as derived from an alignment between the sequence of the *Ciona*KChIP transcript and scaffold 457 of the genomic database for *C. intestinalis* (release version 1.0). Exons are shown as black boxes and numbered in Arabic numerals (1–7). Introns are shown as white boxes and numbered in Roman numerals (I–VI). Intron and exon sizes (in bp) are indicated, respectively, above or below the diagram and are drawn approximately to scale. The 3′-UTR region is represented by box shaded in grey. The 5′-UTR region is delimited by a discontinuous line to indicate that its sequence was not determined in this study.

and *Ciona*KChIP. The *Ciona*Kv4 gene is encoded in ~17.8 kb, of which 2.4 kb encode the ORF. The first exon (exon 0) encoded the first amino acids of the N terminus. The second exon (exon 1), 1070 bp in length, coded most of the channel protein, including the T1 domain, trans-membrane domains S1–S5, and the first part of the pore domain. The second intron interrupted the sequence of the K^+ selectivity filter motif (GYG), since the last base pair of the second exon and the first two base pairs of the third exon encoded the first G of this motif. The second part of the pore region and the S6 trans-membrane domain were encoded by exon 2. Exons 3–5 encoded parts of the C-terminal cytoplasmic domain. The last exon (exon 6), encoded the rest of the C terminus of *Ciona*Kv4, and contained the stop codon (TAG) and the 3′-UTR sequence.

Fig. 2 shows an alignment between the predicted amino acid sequences of *Ciona*Kv4 and selected vertebrate and invertebrate Kv4 channels. The six trans-membrane domains (S1–S6), the pore region, and the first ~23 amino acids of the N terminus of all Kv4 channels showed high sequence similarity. The C-terminal motif PTPP, which is involved in the interaction of Kv4 channels with filamin and is located ~30 amino acids upstream of the C termini of mammalian Kv4 channels (Petrecca et al., 2000), was not found in *Ciona*Kv4, although *Ciona*Kv4 shares the first residue of this motif (P) and the preceding residue (I) with all mammalian Kv4 channels (residues 651–652 in *Ciona*Kv4, Fig. 2). The conserved di-leucine motif, consisting of 16 amino acids that span positions 474–489 and is involved in the targetting of membrane proteins (Rivera et al., 2003), was also found in *Ciona*Kv4 (Fig. 2). The C-terminal domain of *Ciona*Kv4 and the N terminus contained, respectively, two and one putative sites for phosphorylation by cAMP-dependent protein kinase A (PKA). Additionally, the N terminus of *Ciona*Kv4 contained four sites for phosphorylation by protein kinase C (PKC); another four putative sites for PKC phosphorylation were found in the C terminus; and another such site was found in the intracellular loop between membrane-spanning domains S4 and S5.

*Ciona*KChIP was encoded in ~7 kb of genomic DNA, of which the ORF occupied ~0.7 kb, distributed in seven exons with sizes between 69 and 162 bp (Fig. 1D). Fig. 3 shows an alignment between the deduced amino acid sequences of *Ciona*KChIP and representatives of the four major isoforms of mammalian KChIPs (KChIP1–4). As with other KChIPs, the sequence of the N terminus of *Ciona*KChIP was the most variable region of the protein (An et al., 2000) whereas the sequence corresponding to the C terminus was conserved, containing four EF-hand Ca^{2+}-binding motifs (Kretsinger, 1987). The N terminus of *Ciona*KChIP was encoded by exons 1 and 2. The coding region for the first EF-hand was partitioned between exons 2 and 3. Similarly, the codons for the second and the third EF-hands were partitioned between exons 4 and 5 (second EF-hand), and between exons 5 and 6 (third EF-hand). The fourth EF-hand was encoded by exon 6 and the last section of the C-terminus was coded by exon 7. A Prosite scan of *Ciona*KChIP suggested the location of six putative sites for PKC phosphorylation but no sites for PKA phosphorylation (Fig. 3).

Phylogenetic position of CionaKv4 and CionaKChIP

In the phylogenetic tree shown in Fig. 4A, rooting with the cnidarian Kv4 sequences resolved the arthropod and chordate Kv4 channels into sister groups. *Ciona*Kv4 and *Halocynthia* Kv4 (TuKv4; Nakajo et al., 2003) formed a single clade, as would be expected. This tunicate clade is the sister group to the clade containing the Kv4.1, Kv4.2 and Kv4.3 paralogues from vertebrates, indicating that the duplication and divergence that gave rise to the three vertebrate Kv4 channels occurred after the divergence of the vertebrate lineage from the tunicate lineage. In the phylogenetic tree shown in Fig. 4B, the single *Ciona*KChIP branched basal to the four mammalian KChIP isoforms. This tree indicated that there is a 99% likelihood that the KChIP1 isoform is the sister group of the other three isoforms. However, the phylogenetic relationships between the KChIP isoforms 2, 3 and 4 were unclear, with posterior probabilities of approximately 50–60%. There was strong support for the presence of all four isoforms in the common ancestor of modern fish (represented by zebrafish) and the tetrapods (represented by human, mouse, rat and chicken). All of the vertebrate KChIP sequences partitioned robustly into one of the four paralogous families, indicating that the paralogues all originated prior to the origin of the vertebrate clade.

Activation properties of CionaKv4 and an N-deletion mutant of CionaKv4 (ntCionaKv4) in the presence and absence of CionaKChIP

*Ciona*Kv4 channels conducted transient A-type currents (Fig. 5A), whereas currents mediated by *Ciona*Kv4 channels in the presence of *Ciona*KChIP subunits displayed considerably slower inactivation during depolarizing pulses lasting 0.5 s (Fig. 5B). The amplitudes of the currents produced by *Ciona*Kv4 channels co-expressed with *Ciona*KChIP subunits were larger than for *Ciona*Kv4 channels alone, even though half the amount of *Ciona*Kv4 cRNA was injected for co-expression experiments (Figs 5A,B, 6Ai). For example, the average peak amplitudes of the currents produced by *Ciona*Kv4 and *Ciona*Kv4/KChIP for a test pulse to +50 mV

Fig. 2. Alignment and sequence comparison of Kv4 channels from diverse metazoans. Alignment of the deduced amino acid sequence of the three mammalian Kv4 isoforms (Kv4.1, Kv4.2 and Kv4.3), their tunicate homologues (*Ciona*Kv4 and TuKv4), lobster *Shal* (lShal) and jellyfish *Shal* (jShal). T-Coffee software (Notredame et al., 2000) was used to align these sequences, with the following GenPept. accession numbers: *Ciona*Kv4, AAS00646; TuKv4, BAC53863; Kv4.1, 27436981; Kv4.2, 9790093; Kv4.3, 6653655; lShal, AAA81592; jShal, AAB39750. Residues that are identical for at least four of the seven channels are shown in reverse lettering (white on black). Membrane-spanning domains S1–S6, the pore region and the N terminus are underlined. Arrows indicate exon/intron boundaries for *Ciona*Kv4 only. The di-leucine motif is labelled. Putative phosphorylation sites for cAMP-dependent protein kinase (PKA) and protein kinase C (PKC) are indicated by filled circles and open circles, respectively.

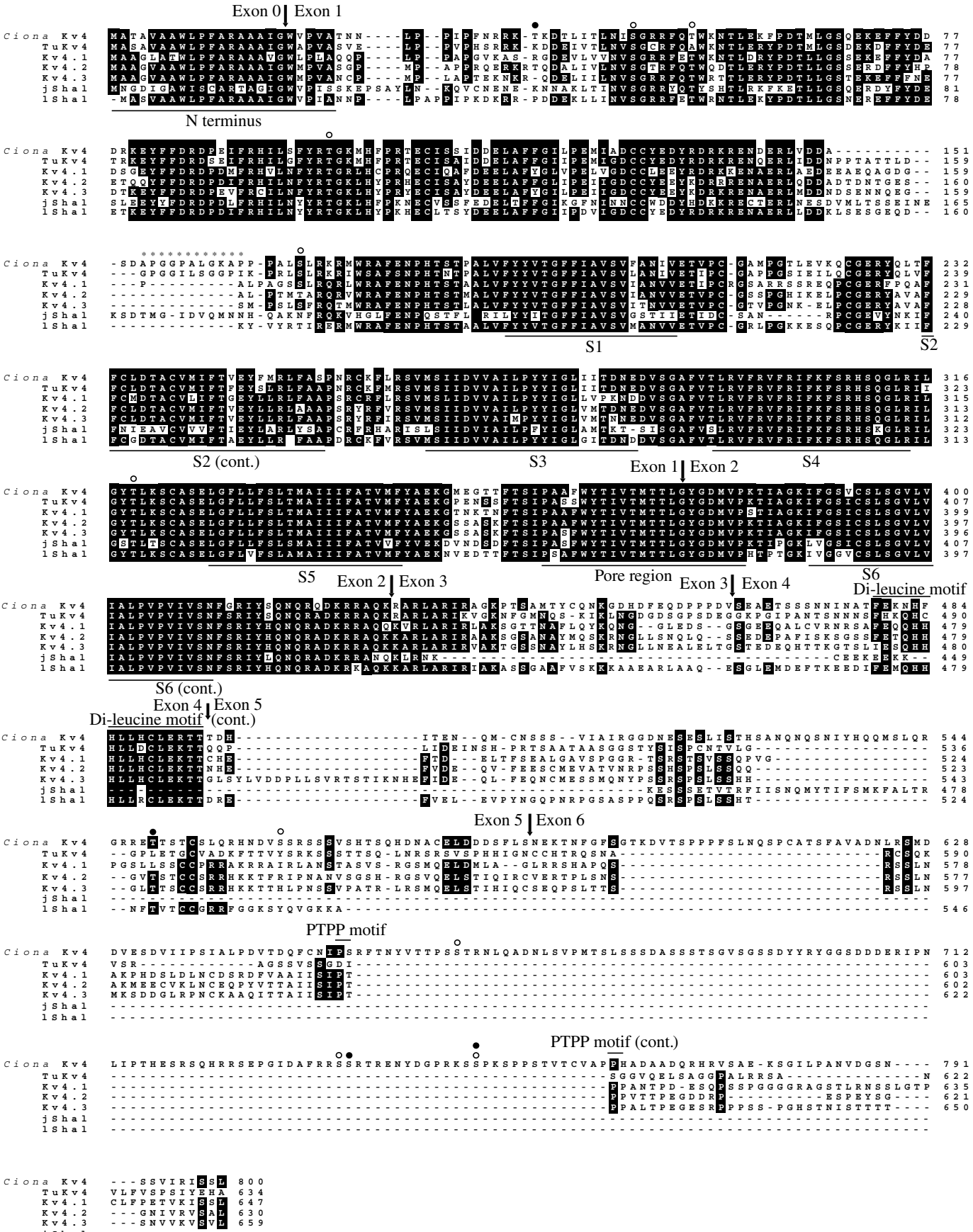

Fig. 2. See previous page for legend.

from a holding potential of –100 mV were 207±27 pA and 867±62 pA, respectively (P<0.0001, Welch t-test). Deletion of the N terminus (amino acids 2–32) of *Ciona*Kv4 also increased the average current amplitude significantly (Figs 5C, 6Aii), but to a lesser extent than when this channel was co-expressed with *Ciona*KChIP (Figs 5D, 6Aiii). For instance, average currents produced by nt*Ciona*Kv4 channels during a pulse to +50 mV had an average peak of 370±65.2 pA compared with 207±27 pA for *Ciona*Kv4 alone (P<0.05, Welch t-test). Addition of *Ciona*KChIP did not affect peak current amplitude of nt*Ciona*Kv4 channels, which lacked the N terminus, since the average peak current of nt*Ciona*Kv4 channels in the presence of *Ciona*KChIP subunits (432±97) was not significantly different (P>0.05, Student t-test) from the average peak amplitude of currents produced by nt*Ciona*Kv4 channels alone (370±65.2 pA), as shown in Fig. 6Aiii.

In all cases, with or without N-terminal truncation and with or without co-expression of KChIP, current levels reached a plateau at stimulation voltages above +50 mV, indicating that conductance decreases above this voltage. The mechanism for this decrease in conductance is unknown. We speculate that the outward current is inhibited at higher depolarization voltages by blocking of the internal face of the ion pore by a positively charged component of the cytoplasm. If the block is similar to Mg^{2+} or polyamine blocking of K_{ir} channels then the affinity of the cytoplasmic blocker must be lower than that seen for polyamine block of K_{ir} channels since blockage of *Ciona*Kv4 does not appear until + 50 mV.

The average time constant of activation of currents produced by *Ciona*Kv4 channels during a pulse to +50 mV (3.4±0.2 ms) was not affected by the presence of *Ciona*KChIP (3.3±0.2 ms), as shown in Fig. 6Bi (P>0.05, Student t-test). The voltage-dependence of the time constant for activation was similar for channels expressed alone or with *Ciona*KChIP, increasing by e-fold every 29 or 33 mV, respectively. Deletion of amino acids 2–32 from *Ciona*Kv4 channels was also without effect on the rate of activation, since the average time constant of activation of currents produced by this N-terminally deleted *Ciona*Kv4 channel was 3.2±0.3 ms (P>0.05, Student t-test). The voltage-dependence of activation kinetics was similar for *Ciona*Kv4 and nt*Ciona*Kv4 channels, increasing by a factor of e for every 26 or 29 mV of voltage change, respectively (Fig. 6Bii). Activation kinetics of nt*Ciona*Kv4 in the presence of *Ciona*KChIP was 3.5±0.3 ms, which was not significantly different from the value for nt*Ciona*Kv4 alone (P>0.05, Student t-test). Interestingly, the voltage-dependence of activation kinetics was different for nt*Ciona*Kv4 channels alone (e-fold increase every 26 mV) than when co-expressed with *Ciona*KChIP (e-fold increase every ~37 mV), which suggests that *Ciona*KChIP slightly decreased the voltage

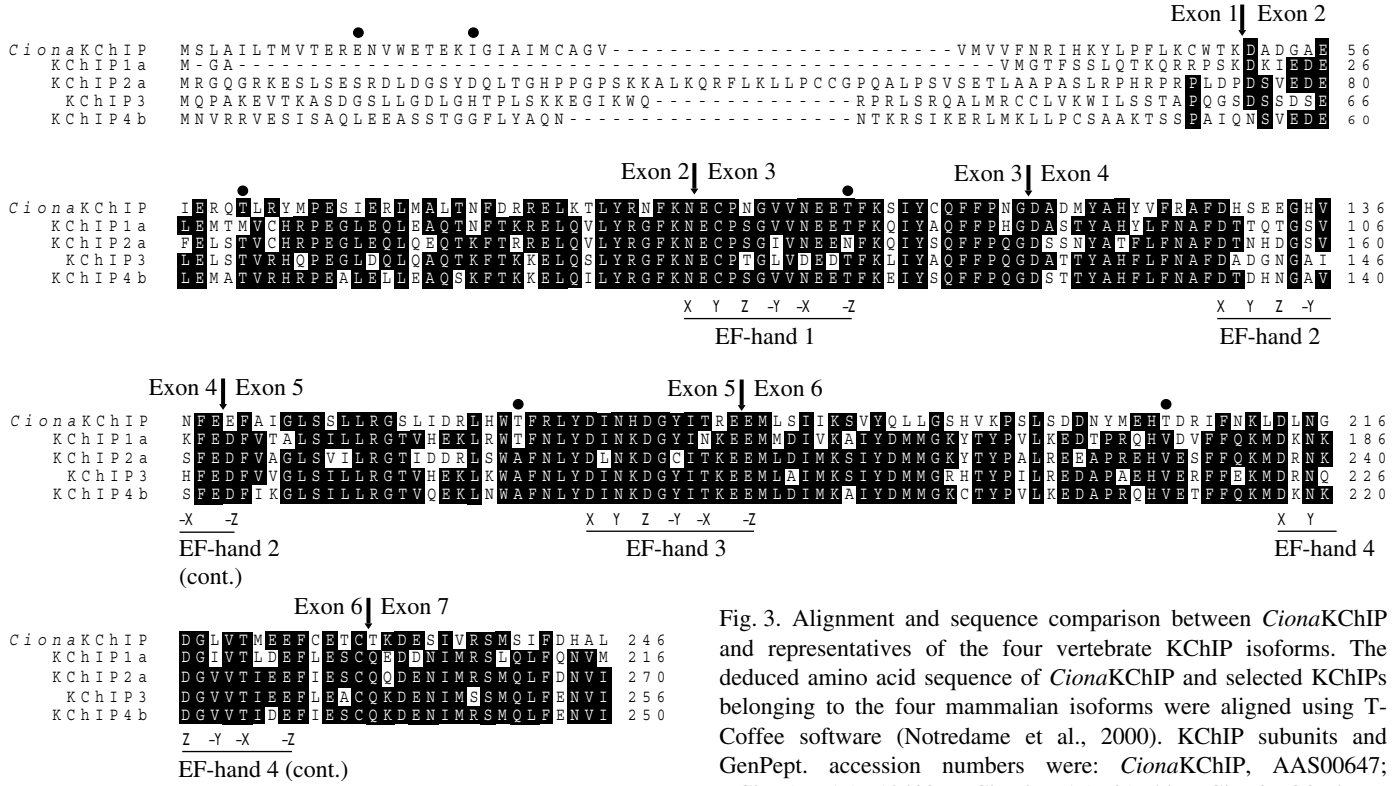

Fig. 3. Alignment and sequence comparison between *Ciona*KChIP and representatives of the four vertebrate KChIP isoforms. The deduced amino acid sequence of *Ciona*KChIP and selected KChIPs belonging to the four mammalian isoforms were aligned using T-Coffee software (Notredame et al., 2000). KChIP subunits and GenPept. accession numbers were: *Ciona*KChIP, AAS00647; KChIP1a, AAL12489; KChIP2a, AAF81755; KChIP3, Q9Y2W7; KChIP4b, NP_079497. Residues that are identical for at least three of the five KChIPs are shown in reverse lettering (white on black). The positions of the four EF-hands are underlined and labelled below the alignment. X,Y,Z,–Y,–X,–Z are the residues that coordinate Ca^{2+} (Bairoch and Cox, 1990). Arrows indicate exon/intron boundaries for *Ciona*KChIP only. Putative phosphorylation sites for protein kinase C (PKC) are indicated by filled circles.

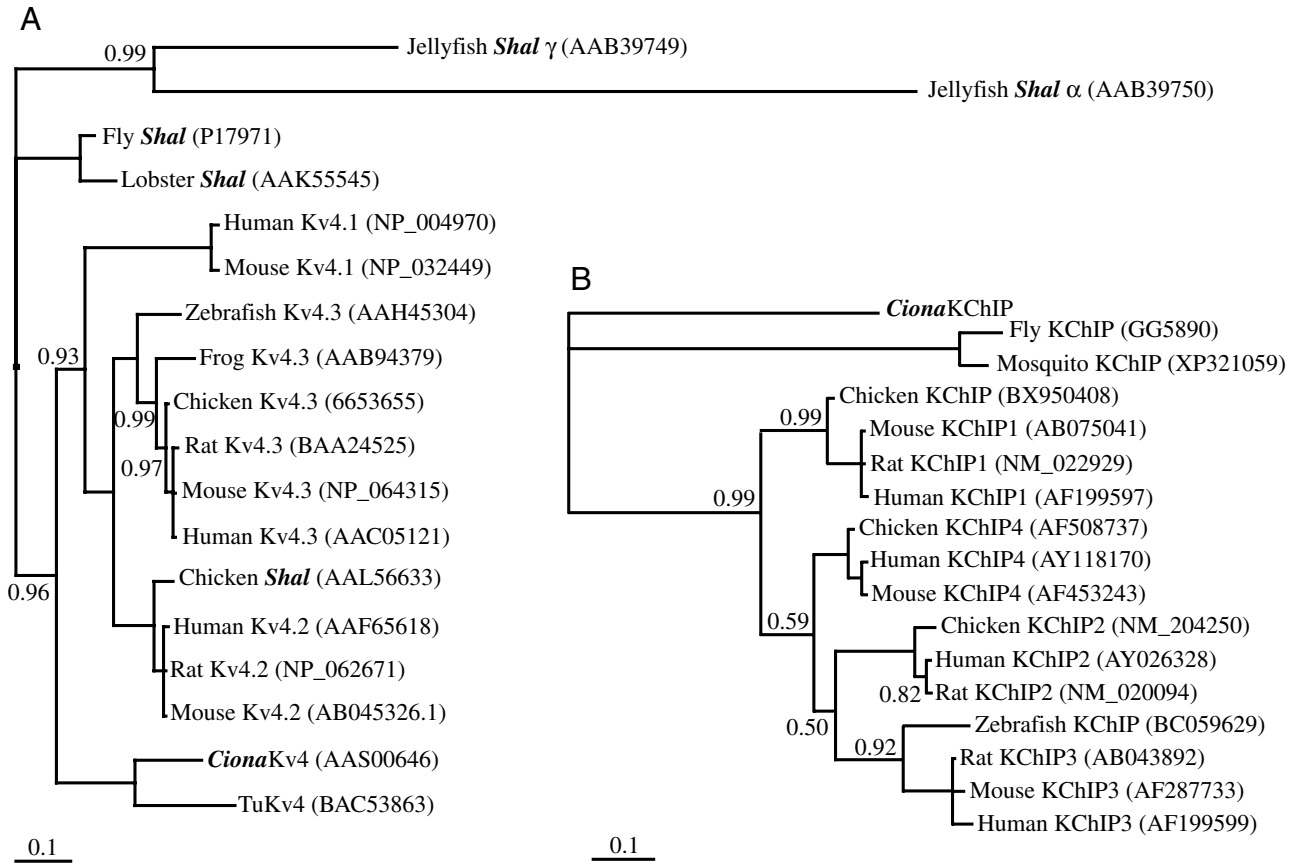

Fig. 4. Phylogenetic relationships of *Ciona*Kv4 and *Ciona*KChIP. (A) Phylogenetic relationships of Kv4 channels from different species. Two cnidarian Kv4 channels were used as an out-group to polarize the relationships of the other channels. The two arthropod channels, Fly *Shal* and Lobster *Shal*, group together as a sister group to the chordate channels. *Shal* and *Ciona* are indicated in bold type. The two tunicate channels, from *Halocynthia roretzi* and *Ciona intestinalis*, group together and are basal to the clade containing all three paralogues of the vertebrates. All of the vertebrate channels group within one of three paralogous clades, indicating that the three vertebrate Kv4 paralogues were present in the common ancestor of all vertebrates, but not in the common ancestor of vertebrates and tunicates. (B) Phylogenetic relationships of KChIPs from different species. Two arthropod KChIPs that were found in BLAST searches of the genomes of *Drosophila* (fly) and *Anopheles gambiae* (mosquito) were used as an out-group to polarize the relationships of the other KChIPs. Numbers above or below the lines indicate Bayesian posterior probability, calculated with the MrBayes program. Unlabelled nodes have a posterior probability of 1. GenPept. accession numbers of the protein sequences are indicated in parentheses. The scale bars represent a divergence equivalent to an average of a 10% change in amino acids.

sensitivity of activation kinetics of nt*Ciona*Kv4 channels (Fig. 6Biii).

*Ciona*KChIP enhanced activation of *Ciona*Kv4 by decreasing the voltage necessary to activate half the channels (Fig. 6Ci), since first order Boltzmann fits to the relationships between normalized peak conductance *vs* voltage had midpoints ($V_{0.5}$) of –0.5±1.7 mV for *Ciona*Kv4 and –29.2±1.1 mV for *Ciona*Kv4/KChIP (P<0.0001, Student *t*-test). The slope values of the Boltzmann curves were 15.5±0.8 mV/e-fold (*Ciona*Kv4) and 13.4±0.3 mV/e-fold (*Ciona*Kv4/KChIP) (P<0.05, Student *t*-test).

Deletion of the N terminus of *Ciona*Kv4 also shifted the midpoint of activation of *Ciona*Kv4 in the hyperpolarizing direction (Fig. 6Cii). First order Boltzmann fits to normalized peak conductance–voltage relationships had significantly different midpoints of activation ($V_{0.5}$) of –0.5±1.7 mV for *Ciona*Kv4 and –12.3±1.6 mV for nt*Ciona*Kv4 (P<0.0001, Student *t*-test). The slopes for these curves were 15.5±0.8 mV/e-fold and 14.3±0.4 mV/e-fold, respectively (P>0.05, Welch *t*-test).

Deletion of the N terminus eliminated the effects of *Ciona*KChIP on activation midpoint (Fig. 6Ciii). The $V_{0.5}$ of first order Boltzmann fits to the conductance–voltage relationships were –15.2±1.3 mV for nt*Ciona*Kv4 in the presence of *Ciona*KChIP (–12.3±1.6 mV for nt*Ciona*Kv4 alone, P>0.05, Student *t*-test). The slope factors of these fits were 14.3±0.4 mV/e-fold for nt*Ciona*Kv4 channels expressed alone, and 13.4±0.2 mV/e-fold for nt*Ciona*Kv4 channels co-expressed with *Ciona*KChIP subunits (P>0.05, Student *t*-test).

All the biophysical parameters determined in this study are summarized in Table 1.

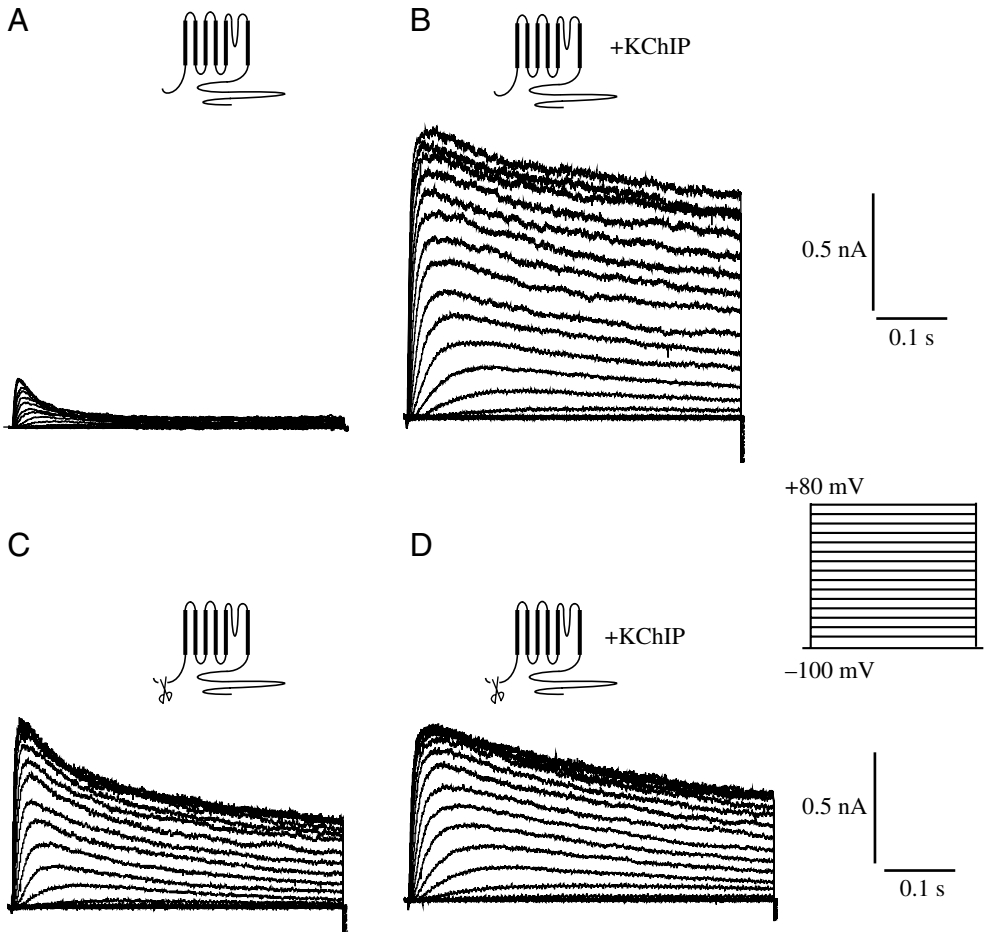

Fig. 5. Currents produced by *Ciona*Kv4 and an N-terminal deleted mutant of *Ciona*Kv4 (nt*Ciona*Kv4) in the presence and absence of *Ciona*KChIP. (A) Representative currents from *Ciona*Kv4 channels expressed alone. (B) Currents produced by *Ciona*Kv4 co-expressed with *Ciona*KChIP. (C) Currents produced by nt*Ciona*Kv4 channels expressed alone. (D) Currents produced by nt*Ciona*Kv4 co-expressed with *Ciona*KChIP. All recordings were obtained using the macro-patch technique. Currents were evoked by depolarizing the macro-patches for 0.5 s from a holding potential of –100 mV to +80mV in 10 mV steps. The form of the stimulus protocol is given on the right.

Inactivation and recovery from inactivation properties of CionaKv4 and an N-deletion mutant of CionaKv4 (ntCionaKv4) in the presence/absence of CionaKChIP

The decaying phase of *Ciona*Kv4 currents obtained with test pulses between +20 mV and +80 mV was well fitted by a double exponential function with fast (τ_1) and slow (τ_2) time constants of inactivation. Currents produced by *Ciona*Kv4/KChIP complexes inactivated more slowly than currents produced by *Ciona*Kv4 channels (Fig. 5B). The decay phases of the currents produced by *Ciona*Kv4/KChIP complexes were well fitted with single exponential functions, whose single inactivation time constants were larger than the slow inactivation time constants of currents produced by *Ciona*Kv4 channels (Fig. 7Ai and Table 1). For instance, the double exponential fit to the decay of currents produced by *Ciona*Kv4 in response to a pulse to +50 mV had a fast time constant of 26±2 ms, which contributed to ~82% of total current decay, and a slow time constant of 147±26 ms, which contributed to ~18% of the current decay. However, a single exponential fit to the inactivation phase of currents conducted by *Ciona*Kv4/KChIP complexes at the same potential had a time constant of 291±42 ms.

The decaying phase of currents produced by N-terminally deleted *Ciona*Kv4 channels was also well fitted by a double exponential function, but the inactivation time constants were slower than for wild-type channels (Fig. 7Aii) and they contributed equally to total inactivation (Table 1). For instance, the decay phase of nt*Ciona*Kv4 currents during a test pulse to +50 mV was best described by a double exponential function with a fast time constant of 56±6 ms and a slow time constant of 381±50 ms. Interestingly, co-expression of nt*Ciona*Kv4 channels with *Ciona*KChIP subunits slowed inactivation kinetics relative to those for nt*Ciona*Kv4 channels alone (Fig. 5D). The decaying phases of these currents were best fitted with single exponential functions, whose time constant was similar to that from untrucated *Ciona*Kv4 channels expressed with *Ciona*KChIP (Fig. 7Aiii and Table 1). These results demonstrate that *Ciona*KChIP still forms a functional complex with *Ciona*Kv4 channels that lack the N terminus.

Since Kv4 channels inactivate mostly from the closed state (Bahring et al., 2001a), we hypothesized that *Ciona*KChIP slowed inactivation kinetics of *Ciona*Kv4 channels by interfering with channel closure. To address this question, we measured and compared the kinetics of tail currents produced by *Ciona*Kv4 channels and *Ciona*Kv4/KChIP complexes in response to re-polarizing pulses from –160 to –110 mV delivered after a brief (10–15 ms) depolarizing pulse to +50 mV, which would activate a maximum number of channels. Our results suggest that channel closing of *Ciona*Kv4 channels is indeed inhibited by *Ciona*KChIP subunits

(Fig. 7Bi). For example, during a re-polarizing pulse to –130 mV, *Ciona*Kv4 tail currents deactivated with a time constant of 4.1±0.3 ms, whereas *Ciona*Kv4/KChIP tail currents deactivated with a time constant of 8.3±0.4 ms. These values were significantly different (P<0.0001, Welch t-test). Deletion of the N terminus of *Ciona*Kv4 also slowed closure kinetics (Fig. 7Bii), indicating that this domain of *Ciona*Kv4 has a role in accelerating channel closure. For example, during a pulse to –130 mV, currents produced by nt*Ciona*Kv4 deactivated with a time constant of 5.7±0.6 ms, which was significantly slower (P<0.05, Welch t-test) than for wild-type channels (4.1±0.3 ms). The N terminus of *Ciona*Kv4 seems to be required for modulation of closing kinetics by *Ciona*KChIP because deactivation time constants of tail currents produced by nt*Ciona*Kv4 channels and nt*Ciona*Kv4/KChIP complexes were not significantly different (Fig. 7Biii). For example, at the

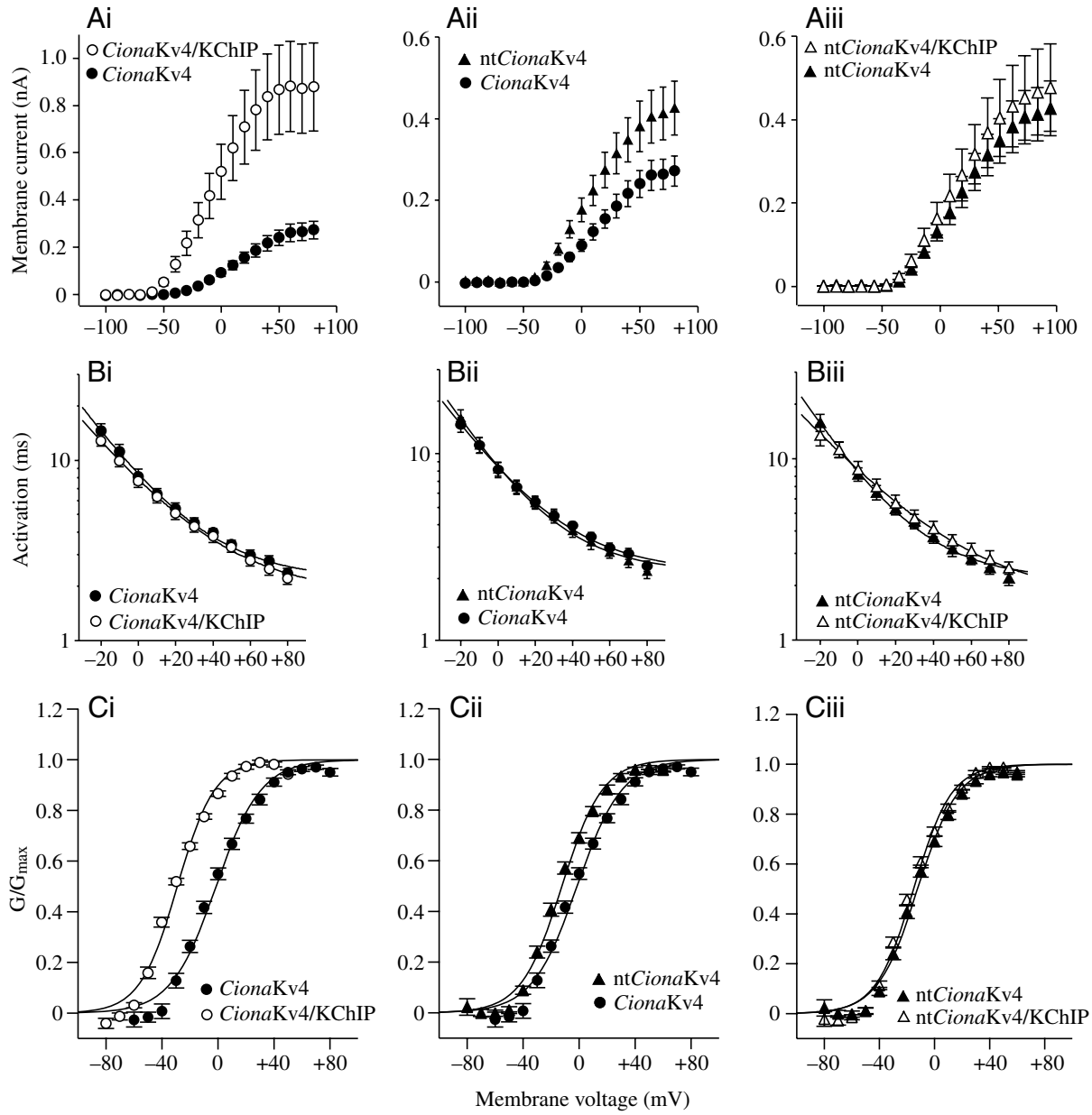

Fig. 6. Activation properties of *Ciona*Kv4 and an N-terminal deletion mutant of *Ciona*Kv4 (nt*Ciona*Kv4) in the presence and absence of *Ciona*KChIP. (A) Comparison between current–voltage relationships for *Ciona*Kv4 alone and in the presence of *Ciona*KChIP (Ai), *Ciona*Kv4 and nt*Ciona*Kv4 (Aii), and nt*Ciona*Kv4 alone or with *Ciona*KChIP (Aiii). N=17. (B) Comparison between the time constants of macroscopic activation (τ activation)–voltage relationships for *Ciona*Kv4 alone or in the presence of *Ciona*KChIP (Bi), for *Ciona*Kv4 and nt*Ciona*Kv4 (Bii), and for nt*Ciona*Kv4 alone or with *Ciona*KChIP (Biii). Solid curves represent single exponential fits to these relationships. N=12. (C) Comparison between normalized peak conductance–voltage relationships for *Ciona*Kv4 alone or with *Ciona*KChIP (Ci), for *Ciona*Kv4 and nt*Ciona*Kv4 (Cii), and for nt*Ciona*Kv4 alone or with *Ciona*KChIP (Ciii). N=17. Solid curves represent first order Boltzmann fits of the averaged data. nt*Ciona*Kv4 symbolizes *Ciona*Kv4 channels lacking N-terminal amino acids 2–32. Values are means ± s.e.m.

re-polarizing voltage of –130 mV, the deactivation time constant for nt*Ciona*Kv4 in the presence of *Ciona*KChIP was 6.5±0.6 ms, which was not significantly different (P>0.05, Student t-test) from the average deactivation time constant for nt*Ciona*Kv4 channels expressed alone (5.7±0.6 ms).

Addition *of Ciona*KChIP shifted the midpoint of steady-state inactivation of *Ciona*Kv4 to the left (Fig. 7Ci). Midpoints of single order Boltzmann fits to steady-state inactivation curves of *Ciona*Kv4 and *Ciona*Kv4/KChIP were –72±2 mV for *Ciona*Kv4 and –88±2 mV for *Ciona*Kv4/KChIP (P<0.001, Student t-test). The slope factors of these Boltzmann fits to steady-state inactivation were also significantly different: 3.6±0.2 mV/e-fold for *Ciona*Kv4 and 4.3±0.2 mV/e-fold for *Ciona*Kv4/KChIP (P<0.001, Student t-test). The N terminus of *Ciona*Kv4 does not appear to contribute to steady state inactivation (Fig. 7Cii) since midpoints of inactivation of N-terminally deleted channels (–73±2 mV) were not significantly different (P>0.05, Student t-test) from inactivation midpoints of wild-type channels (–72±2 mV). The slopes of the steady-state inactivation curves were not significantly different (P>0.05, Student t-test): 3.6±0.2 mV/e-fold for *Ciona*Kv4 and 3.7±0.2 mV/e-fold for nt*Ciona*Kv4. However, the effect of *Ciona*KChIP on steady-state inactivation parameters was dependent on the N terminus of *Ciona*Kv4, since deletion of this domain abolished these effects (Fig. 7Ciii). Midpoints of inactivation were –73±2 mV for nt*Ciona*Kv4 and –74±2 mV for nt*Ciona*Kv4/KChIP. Slope factors were 3.7±0.2 for nt*Ciona*Kv4 and 4.1±0.3 for nt*Ciona*Kv4/KChIP (P>0.05, Student t-test, for both midpoint and slope values).

The rate of recovery from inactivation of *Ciona*Kv4 channels at –100 mV was also affected by *Ciona*KChIP (Fig. 7Di). Recovery from inactivation was measured as the fractional recovery of current as a function of time at –100 mV. This relationship was well fitted by a single exponential function with recovery time constants from inactivation (τ_{rec}) of 387.4±46.6 ms for *Ciona*Kv4 and 330.6±49.5 ms for nt*Ciona*Kv4 (P>0.05, Student t-test), indicating that the N-terminal peptide sequence alone is not a significant factor in recovery (Fig. 7Dii). The recovery of unmutated *Ciona*Kv4 channels was significantly slowed by the presence of *Ciona*KChIP, with a time constant of recovery of 927±47 ms (Fig. 7Di and Table 1). The recovery of the nt*Ciona*Kv4 channel was also slowed significantly by the presence of *Ciona*KChIP, with a time constant of recovery of 587±76 ms (Fig. 7Diii and Table 1), although the effect was less than on the unmutated *Ciona*Kv4.

Discussion

Since orthologous transcription factors control the early stages of cardiac morphogenesis in invertebrates (Bodmer, 1993), early chordates (Komuro and Izumo, 1993; Holland et al., 2003) and vertebrates (Davidson and Levine, 2003), it is reasonable to suppose that hearts are homologous across chordate phylogeny (Romer and Parsons, 1986) and also within certain invertebrate lineages. Therefore, it was not surprising that the message for a Kv4 channel was present in RNA extracted from the heart of the tunicate *Ciona intestinalis*, since these channels are known to mediate a transient current responsible for the 'notch' in cardiac action potentials from fish to mammals (Dixon et al., 1996; Brahmajothi et al., 1999; Nurmi and Vornanen, 2002; Roden et al., 2002). Similarly modulation of Kv4 mediated currents by KChIP and analogous calcium-binding accessory subunits is common across the Metazoa (Rosati et al., 2001; Zhang et al., 2003). Although genes for KChIP subunits have been identified by BLAST searches in the genomes of *Drosophila* and *Anopheles*, *Ciona*KChIP is the first KChIP subunit from an invertebrate or non-vertebrate chordate that has been cloned and characterized.

Comparing the genomic structure of CionaKv4 and CionaKChIP with their mammalian counterparts

The genomic structure of *Ciona*Kv4 (Fig. 1B) was similar to the genomic structures of the three mammalian Kv4 channel genes, which have been previously characterized (Isbrandt et al., 2000). Interestingly, the *Ciona*Kv4 gene contains an additional intron that partitions the codons for the first 17 amino acids onto an additional exon. For comparison, exons 1–7 of *Ciona*Kv4 were numbered 0–6 because the boundaries

Fig. 7. Inactivation properties of *Ciona*Kv4 and an N-terminal deletion mutant of *Ciona*Kv4 (nt*Ciona*Kv4) in the presence/absence of *Ciona*KChIP. (A) Comparison of the time constant of macroscopic inactivation (τ inactivation)–voltage relationships for (Ai) *Ciona*Kv4 alone (wt) or in the presence of *Ciona*KChIP (wt+), (Aii) *Ciona*Kv4 (wt) and nt*Ciona*Kv4 (nt), and (Aiii) nt*Ciona*Kv4 alone (nt) or with *Ciona*KChIP (nt+). τ1 (circles) and τ2 (squares) are the time constants of the fast and slow components of inactivation, respectively, of *Ciona*Kv4 (solid symbols) or nt*Ciona*Kv4 (open symbols) currents. τ (diamonds) is the time constant of the single component of inactivation of *Ciona*Kv4/KChIP (solid diamonds) or nt*Ciona*Kv4/KChIP (open diamonds). All inactivation kinetics appear to be insensitive to voltage. N=15. (B) Comparison of the time constant of deactivation (τ deactivation)–voltage relationships for (Bi) *Ciona*Kv4 alone or in the presence of *Ciona*KChIP, (Bii) *Ciona*Kv4 and nt*Ciona*Kv4, and (Biii) nt*Ciona*Kv4 alone or with *Ciona*KChIP. N=16. (C) Comparison of the steady-state inactivation curves for (Ci) *Ciona*Kv4 alone or with *Ciona*KChIP, (Cii) *Ciona*Kv4 and nt*Ciona*Kv4, and (Ciii) nt*Ciona*Kv4 alone or with *Ciona*KChIP. Solid curves represent first order Boltzmann fits of the averaged data. Steady-state inactivation was determined by measuring the peak current evoked with a depolarizing pulse to +50 mV as a function of the voltage of a preceding 10 s prepulse test (between –130 and –30 mV). N=8. (D) Comparison of the rates of recovery from inactivation for (Di) *Ciona*Kv4 alone or in the presence of *Ciona*KChIP, (Dii) *Ciona*Kv4 and nt*Ciona*Kv4, and (Diii) nt*Ciona*Kv4 alone or in the presence of *Ciona*KChIP. N=8. A double-pulse protocol was used with a test pulse to +50 mV lasting 1 s separated by a recovery period (at –100 mV) of increasing duration (50–2000 ms) from a second test pulse to +50 mV. The currents evoked by the second pulse (I_0) were normalized to the currents produced by the first pulse (I) and plotted against the duration of the interpulse interval. Solid curves represent single exponential fits to the data. Values are means ± s.e.m.

and relative sizes of exons 2–7 correspond to exons 1–6 of mammalian Kv4 channels. The exon that encodes the first 17 amino acids of *Ciona*Kv4 is referred to as 'exon 0' and is located ~8 kb upstream of exon 1 (Fig. 1B). As in mammalian Kv4 channel genes, exon 1 of *Ciona*Kv4 encodes the transmembrane domains S1–S5 and the first part of the pore domain of *Ciona*Kv4, exon 2 encodes the second part of the pore and transmembrane domain S6, and exons 3–6 encode the C terminus. The intron between exons 1 and 2 in *Ciona*Kv4 interrupts the coding sequence of the K^+ selectivity sequence

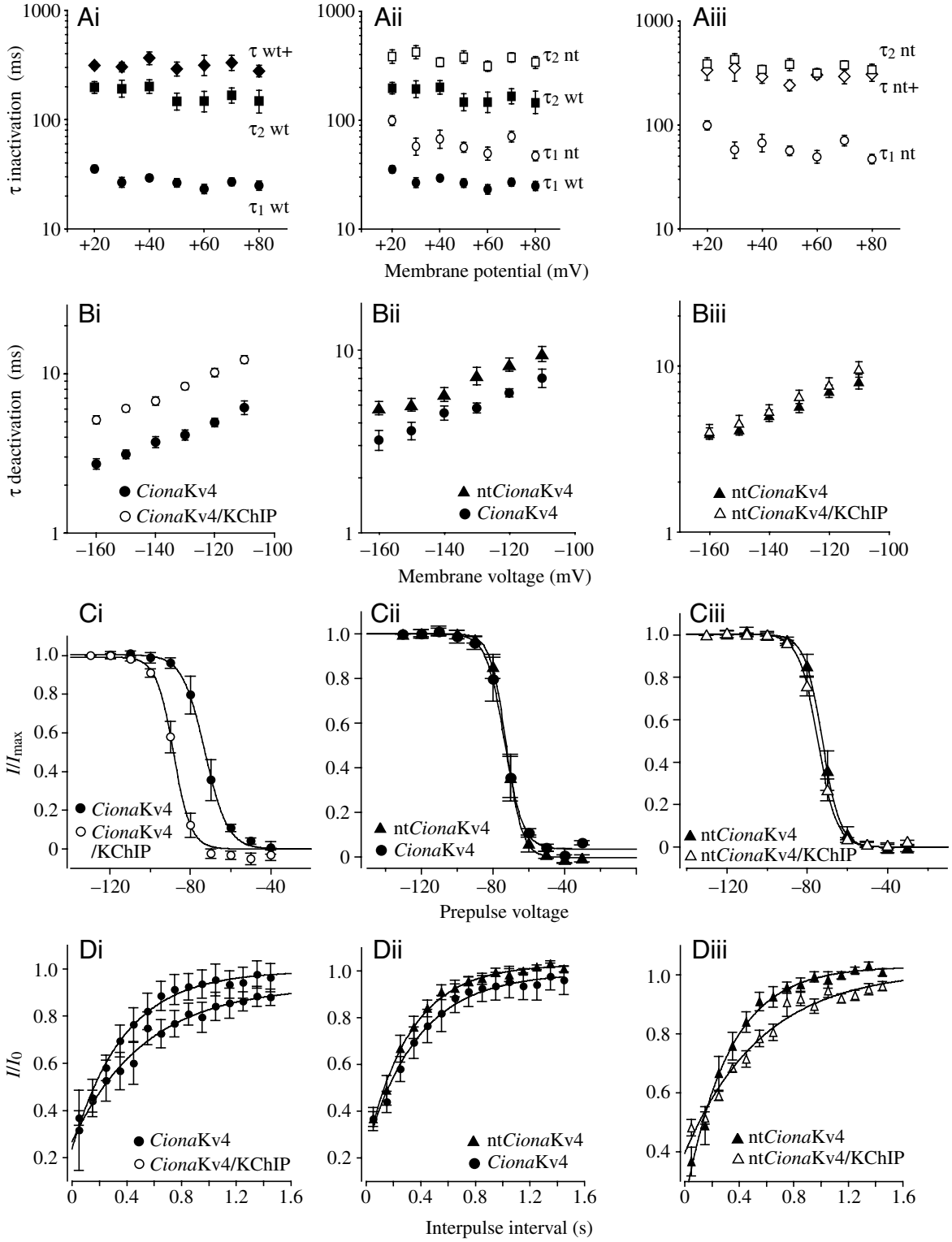

Fig. 7. See previous page for legend.

GYG at exactly the same position as the equivalent intron of mammalian Kv4 genes. The sixth exon of *Ciona*Kv4 is larger in this gene than in its mammalian counterparts, encoding a comparatively longer C terminus.

Comparison between the genomic structures of *Ciona*KChIP (Fig. 1D) and the KChIPs cloned from several mammalian species revealed that most exon/intron boundaries of KChIPs are highly conserved. For example, the last exon of *Ciona*KChIP, KChIP2 and KChIP3 are identical in length (Decher et al., 2004; Spreafico et al., 2001). Each of the EF-hands 1 to 3 of *Ciona*KChIP is encoded by two exons, as in KChIP3, and the partition of these three EF-hands into two exons occurs in the same positions in *Ciona*KChIP and KChIP3. The fourth EF-hand is similarly encoded in a single exon in *Ciona*KChIP, KChIP2 and KChIP3 (Decher et al., 2001; Spreafico et al., 2001). The number of exons that encode the different mammalian KChIPs is variable, since numerous splice variants from a single KChIP gene are possible; for example, the gene encoding KChIP2 subunits can be spliced differently to produce at least eight isoforms that differ in their N terminus: KChIP2a (An et al., 2000), KChIP2b (Bähring et al., 2001b), KChIP2c (Decher et al., 2001), KChIP2d (Patel et al., 2002), KChIPs 2e-g (Decher et al., 2004), and KChIP2t (Deschênes et al., 2002). The fact that *Ciona*KChIP is encoded by several exons, in a similar fashion to the mammalian KChIP isoforms (Fig. 1D), suggests that several splice variants of *Ciona*KChIP are possible, although only one variant was detected in our experiments. Although most splice variants of KChIPs differ in their N termini, variants that differ in their C termini have been also cloned (Decher et al., 2004). Our results suggest that splice variants of *Ciona*KChIP that differ in their C termini are not expressed, or are expressed at very low levels in the heart of *Ciona intestinalis*, because otherwise these would have been detected with the 3′-RACE assay. Since we did not perform a 5′-RACE assay it is possible that alternatively spliced variants of *Ciona*KChIP with one or more alternative N-terminal exons, variants containing the information encoded by possible additional exons, or splice variants without an N terminus, similar to the minimal isoform KChIP2d (Patel et al., 2002), are expressed in the heart of *C. intestinalis*. However, we can suggest that splice variants that do not contain the information of one or more of exons 2–5 are not expressed, or expressed at relatively low levels, otherwise it is likely that these would have been detected when amplifying the ORF of *Ciona*KChIP.

Comparing the function of CionaKv4 and other Kv4 channels

*Ciona*Kv4 produced A-type currents that activated and inactivated with relatively rapid kinetics. The relative contribution of the fast inactivation component (~82%) was comparable to that of lobster *Shal* (Baro et al., 1996), Kv4.2 (Bähring et al., 2001a) and Kv4.3 (Wang et al., 2002), but was significantly greater than the <20% recorded for Kv4.1 channels (Jerng and Covarrubias, 1997). The fast inactivation time constant of *Ciona*Kv4 at 12°C was about 26 ms, similar to lobster *Shal* (~31 ms at 16°C; Baro et al., 1996) and mammalian *Shal* (~23–23°C; Pak et al., 1991). The fact that this inactivating component has a similar time constant at very different temperatures suggests that inactivation kinetics of Kv4 channels are not constrained by temperature. Low Q_{10}

Table 1. *Biophysical parameters determined in this study*

	*Ciona*Kv4		nt*Ciona*Kv4	
Biophysical parameter	–*Ciona*KChIP	+*Ciona*KChIP	–*Ciona*KChIP	+*Ciona*KChIP
I_{peak} (pA) at +50 mV	207±27 (15)	867±62 (17)[a]	370±65.2 (15)	432±97 (15)
τ_{act} (ms) at +50 mV	3.4±0.2 (11)	3.3±0.2 (10)	3.2±0.3 (12)	3.5±0.3 (12)
Inactivation (ms) at +50 mV				
τ_1	26±2 (15)	291±42 (9)	56±6 (15)	240±29 (8)
I_1	82%	100%	49%	100%
τ_2	147±26 (15)	–	381±50 (15)	–
I_2	18%	–	51%	–
τ_{rec} (ms) at –100 mV	387±47 (7)	927±47 (6)[a]	331±51 (8)	587±76 (8)[b]
τ_{deact} (ms) at –130 mV	4.1±0.3 (10)	8.3±0.4 (16)[a]	5.7±0.6 (12)	6.5±0.6 (10)
Steady-state activation (mV)				
$V_{0.5}$	–0.5±1.7 (15)	–29.2±1.1 (17)[a]	–12.3±1.6 (15)	–15.2±1.3 (15)
K	15.5±0.8 (15)	13.4±0.3 (17)	14.3±0.4 (15)	13.4±0.2 (15)
Steady-state inactivation (mV)				
$V_{0.5}$	–72±2 (7)	–88±2 (7)[a]	–73±2 (7)	–74±2 (8)
K	3.6±0.2 (7)	4.3±0.2 (7)[a]	3.7±0.2 (7)	4.1±0.3 (8)

For definitions of parameters, see List of symbols.
[a]Significantly different from *Ciona*Kv4 (P<0.01).
[b]Significantly different from nt*Ciona*Kv4 (0.01<P<0.05).

values are common for marine animals in shallow temperate waters.

The midpoint of activation of *Ciona*Kv4, ~0 mV (Fig. 6Ci and Table 1), is considerably depolarized with respect to that of the Kv4 channel cloned from another tunicate (*Halocynthia*), around –20 mV, as measured from Fig. 2 of Nakajo et al. (2003) and with respect to most mammalian Kv4 channels, approximately –10 to –15 mV (see records for Kv4 family in http://vkcdb.biology.ualberta.ca/). The first N-terminal amino acids of *Ciona*Kv4 are likely involved in regulating membrane expression, since deletion of these residues resulted in increased current amplitude relative to wild-type channels when expressed in *Xenopus* oocytes (Fig. 6Ai). This result mimicked the effect of deleting a similar fragment from mammalian Kv4 channels (Bähring et al., 2001a; Shibata et al., 2003). It has been shown that the hydrophobicity of most of the first ~30 amino acids of Kv4 channels impedes the trafficking of these channels to the membrane (Shibata et al., 2003).

Deletion of amino acids 2–32 of *Ciona*Kv4 slowed the fast component of inactivation approximately twofold (Fig. 7Aii) and slowed deactivation kinetics (Fig. 7Bii). However, the N terminus of *Ciona*Kv4 does not play a role in steady-state inactivation (Fig. 7Cii). These data suggest that the role of the N terminus of *Ciona*Kv4 in inactivation is comparable to the role of the N terminus of Kv4.2 channels, because deleting the first 40 amino acids of Kv4.2 channels had similar effects on the rate of inactivation and steady-state inactivation (Bähring et al., 2001a). The role of the N terminus of Kv4.1 channels is divergent, as its deletion resulted in loss of the fast component of inactivation of this isoform (Pak et al., 1991; Jerng and Covarrubias, 1997). Interestingly, the N terminus of *Ciona*Kv4 also contributes to the voltage-dependence of activation, since deletion of this domain resulted in a significant shift of the activation midpoint by about 12 mV in the hyperpolarizing direction relative to wild-type channels (Fig. 6Cii and Table 1).

Like the N terminus of mammalian Kv4 channels (Bähring et al., 2001), the N terminus of *Ciona*Kv4 is essential for modulation of some channel properties by KChIP subunits, since in the absence of this domain, *Ciona*KChIP did not increase current amplitude, shift midpoint values of activation or inactivation or affect the kinetics of deactivation of *Ciona*Kv4 channels (see below). However, the macroscopic decay of nt*Ciona*Kv4/KChIP currents was slower than the decay of nt*Ciona*Kv4 channels alone. It is likely that *Ciona*KChIP, in addition to interacting with the proximal amino acids of the N terminus of *Ciona*Kv4, also binds to a second domain of the N terminus that was not affected by the deletion performed on *Ciona*Kv4 channels. Mammalian KChIPs interact with at least two domains of the N terminus of Kv4 channels, one within residues 7–11 and another comprising residues 71–90 (Scannevin et al., 2004), and this second binding site is sufficient for binding to KChIPs.

KChIP modulation of current amplitude and activation parameters

As do mammalian KChIP isoforms 1–3 (An et al., 2000), *Ciona*KChIP increased the amplitude of *Ciona*Kv4 currents (Figs 5B, 6Ai). The mammalian KChIP isoforms do not increase the Kv4 current amplitude by a direct effect on single channel conductance (Beck et al., 2002), but by preventing aggregation of their hydrophobic N terminus in the ER that would interfere with folding. Proper folding favours the insertion of Kv4 channels into the plasma membrane and increases their half-life in the membrane (Shibata et al., 2003). This study did not determine whether *Ciona*KChIP increases current amplitude by facilitating proper insertion of these channels in the plasma membrane or by increasing the conductance of *Ciona*Kv4 channels. *Ciona*KChIP shifted the midpoint of activation of *Ciona*Kv4 in the hyperpolarizing direction (Fig. 6Ci), which is consistent with the effect of most mammalian KChIPs (An et al., 2000; Van Hoorick et al., 2003).

KChIP modulation of inactivation

*Ciona*KChIP slowed inactivation of the transient currents produced by *Ciona*Kv4. This was reminiscent of the effects of the mammalian isoform KChIP4a on mammalian Kv4 channels (Holmqvist et al., 2002). The N terminus of KChIP4a [K inactivation suppressor domain (KIS)] is required for its effect on inactivation kinetics (Holmqvist et al., 2002). To determine

A
*Ciona*KChIP MSLAILTMVTERENVWET----EKIGIAIMCAGVVMVVFNRIHK
KChIP4a MNLEGLRMIAVLIVIVLFVKLLEQFGL--IEAGLEDSVEDEL--

B
*Ciona*KChIP MSLAIL---TMVTERENVWETEKIGIAIMCAGVVMVVFNRIHK--
KChIP1a M-GAVMGTFSSLQTKQRRPSKDKIEDEL---EMT-MVCHRPEGLE

C
*Ciona*KChIP M-------SLAI----------LTMVTERENVWETEKIGIAIMCAGVVMVVFNRIHK
KChIP2a MRGQGRKESLSESRDLDGSYDQLT----GHPPGPSKK------------ALKQRFL

D
*Ciona*KCHIP M-----------SLAILTMVTERENVWETEKIGIAIMCAGVVMVVFNRIHK-
KChIP3a MQPAKEVTKASDGSL-----LGDLGHTPLSKKEGIKWQRP--------RLSRQ

Fig. 8. Alignment and sequence comparisons between the N termini of *Ciona*KChIP and representatives of each mammalian KChIP isoform. (A) Alignment between the N termini of *Ciona*KChIP and KChIP4a (GenPept. accession number AAL86766), which contains the K inactivation suppressor domain (KIS). (B) Alignment between the N termini of *Ciona*KChIP and KChIP1a (GenPept. accession number AAL12489). (C) Alignment between the N termini of *Ciona*KChIP and KChIP2a (GenPept. accession number AAF81755). (D) Alignment between the N termini of *Ciona*KChIP and KChIP3a (GenPept. accession number Q9Y2W7). T-Coffee software (Notredame et al., 2000) was used to align these sequences. Residues that are identical for each pair of sequences are boxed.

whether the N terminus of *Ciona*KChIP also has the KIS domain, we aligned the first 40 amino acids of *Ciona*KChIP with the first 40 amino acids of KChIP4a using T-Coffee software (Notredame et al., 2000). The results of this alignment are shown in Fig.·8A. For comparison, we also aligned the first 40 amino acids of *Ciona*KChIP with the first 40 amino acids of representatives of the other vertebrate KChIP subfamilies (KChIP1–3). Interestingly, the N terminus of *Ciona*KChIP was more similar to the N terminus of the KChIP4a isoform than to the N termini of other KChIP isoforms. The alignment between *Ciona*KChIP and KChIP4a revealed that two leucines, at positions 3 and 6 in both subunits, and a methionine, at position 8 also in both subunits, are conserved between KChIP4a and *Ciona*KChIP (Fig. 8A). Other residues that are conserved between the N terminus of KChIP4a and CionaKChIP are a glutamic acid residue and a glycine residue at positions 19 and 22, in *Ciona*KChIP (positions 23 and 26 in KChIP4a), an alanine-glycine motif located at position 28 in *Ciona*KChIP (position 30 in KChIP4a), and a valine residue at position 34 in *Ciona*KChIP (position 32 of KChIP4a; Fig. 8A). These conserved residues may be crucial to the modulation by KChIP subunits on inactivation kinetics. The alignments between *Ciona*KChIP and KChIP2a or KChIP3a had extensive gaps (Fig. 8C,D). The alignment between *Ciona*KChIP and KChIP1a has fewer and smaller gaps for other isoforms, perhaps revealing a closer relationship between the N termini of these two subunits (Fig. 8B).

Most KChIP isoforms either do not affect the midpoint of inactivation (e.g. KChIP1a; Nakamura et al., 2001; Van Hoorick et al., 2003) or shift the midpoint of inactivation in the depolarizing direction (e.g. KChIP2b; Bähring et al., 2001b). However, the splice variant KChIP2g, which has an alternative exon 1 (Decher et al., 2004) and KChIP 1b, which contains the information of an additional exon in its N terminus (Van Hoorick et al., 2003), shifts the midpoint of inactivation in the hyperpolarizing direction as for *Ciona*KChIP (Fig. 7Ci). However, the N termini of these mammalian KChIP splice variants and *Ciona*KChIP are not similar.

KChIP modulation of recovery from inactivation

*Ciona*Kv4 channels required ~1 s to fully recover from inactivation at –100 mV, with a recovery time constant of ~387 ms (Fig. 7D). Similar values have been reported for jellyfish and fly *Shal* (Jegla and Salkoff, 1997) and Kv4.2 (Serôdio et al., 1994) for the same membrane potential. Kv4.1 channels recover fully from inactivation within 300–400 ms at –100 mV (Serôdio et al., 1994), while Kv4.3 channels recover from inactivation relatively rapidly, with recovery time constants of less than 200 ms, also at –100 mV (Dixon et al., 1996). In conclusion, invertebrate and non-vertebrate chordate Kv4 channels, including *Ciona*Kv4, exhibit lower rates of recovery from inactivation than the mammalian Kv4.1 and KvV4.3 channel subtypes, suggesting that relatively slow kinetics of recovery is a primitive feature of Kv4 channels.

The Kv4 channel and the KChIP subunit diversified during vertebrate evolution

Since the mammalian genome contains three Kv4 paralogues and four KChIP paralogues, while the genome of *Ciona intestinalis* contains only one gene for Kv4 channels and a single gene for KChIP subunits, it is probable that both genes duplicated and diverged in the vertebrate lineage during evolution. Current theory states that there were two major genome duplications early in the evolution of the vertebrates (Ohno, 1970). Most vertebrate gene families (81%) are composed of two or three paralogues that derive from a single ancestral gene (Escriva et al., 2002), as is the case for the Kv4 channel gene family. Gene families formed by three paralogues are believed to have lost a fourth paralogue after the second large-scale genomic duplication (Spring, 1997). Since the KChIP gene family has four paralogues in vertebrates, it is unlikely that gene loss occurred after the second large-scale duplication. The pattern of KChIP clades in the vertebrate lineage (Fig. 4B), [A(B(CD))], is not consistent with two successive genome duplications. The fact that this pattern is common within vertebrate gene families composed of four paralogues has been used by Hugues (1999) to argue against two rounds of genomic duplication, as this duplication pattern would have rendered a topology of the form: (AB)(CD). Sidow (1996) has suggested that duplications of single genes or fragments of the genome that were independent of large-scale genomic duplications have played a role in the evolution of the vertebrates and might explain these discrepancies. However, the support values for the two internal branching events in the vertebrate KChIP clade are so low that the relationships of these four paralogues are most reasonably described by an unresolved polytomy rather than either of the specific evolutionary models.

Conclusion

Until this study, invertebrate KChIPs had not been cloned. However it has been shown that crustacean Kv4 channels can be modulated by a mammalian KChIP (Zhang et al., 2003) in a similar fashion to that shown by the effect of *Ciona*KChIP on *Ciona*Kv4 shown in this study. This is the first cloning of a non-vertebrate KChIP, and since tunicates are the earliest diverging chordate clade, these results show that modulation of Kv channels by calcium-binding proteins in vertebrates is an ancient and conserved mechanism.

We conclude that tunicate KChIP subunits modulate expression, voltage sensitivity of gating, and kinetic behavior of tunicate Kv4 channels. Modulation by *Ciona*KChIP requires an intact N terminus of *Ciona*Kv4, as in mammals. *Ciona*KChIP dramatically slowed the rate of inactivation of *Ciona*Kv4 channels, similarly to the vertebrate KChIP4a isoform (Holmqvist et al., 2004) and our comparative analyses may have provided clues as to the N-terminal amino acids in KChIP that are responsible for this action. Our results are also the first report on the molecular nature of excitability in the tunicate myocardium, which may help further our understanding of its physiology and the evolution of hearts. We

suggest that modulation of Kv4 channels by KChIP subunits is a conserved mechanism to modulate cardiac excitability.

List of symbols and abbreviations

E_K	measured potassium equilibrium potential
G_K	potassium conductance
G_{max}	maximal conductance
I_{max}	maximum current
I_0	offset current
I_{peak}	peak measured amplitude
K	slope factor
K_{ir}	inward rectifier potassium channel
KChIP	potassium channel interacting protein
Kv4	voltage-gated potassium channel, *Shal* subtype
t	time
V	voltage
$V_{0.5}$	voltage at which activation/inactivation is half maximal
τ	activation time constant.
τ_{rec}	recovery time constant

References

Amberg, G. C., Koh, S. D., Hatton, W. J., Murray, K. J., Monaghan, K., Horowitz, B. and Sanders, K. M. (2002). Contribution of Kv4 channels toward the A-type potassium current in murine colonic myocytes. *J. Physiol.* **544**, 403-415.

An, W. F., Bowlby, M. R., Betty, M., Cao, J., Ling, H. P., Mendoza, G., Hinson, J. W., Mattsson, K. I., Strassle, B. W., Trimmer, J. S. et al. (2000). Modulation of A-type potassium channels by a family of calcium sensors. *Nature* **403**, 553-556.

Bähring, R., Boland, L. M., Varghese, A., Gebauer, M. and Pongs, O. (2001a). Kinetic analysis of open- and closed-state inactivation transitions in human Kv4. 2 A-type potassium channels. *J. Physiol.* **535**, 65-81.

Bähring, R., Dannenberg, J., Peters, H. C., Leicher, T., Pongs, O. and Isbrandt, D. (2001b). Conserved Kv4 N-terminal domain critical for effects of Kv channel-interacting protein 2.2 on channel expression and gating. *J. Biol. Chem.* **276**, 23888-23894.

Bairoch, A. and Cox, J. A. (1990). EF-hand motifs in inositol phospholipids-specifc phospholipase C. *FEBS Lett.* **269**, 454-456.

Baro, D. J., Coniglio, L. M., Cole, C. L., Rodriguez, H. E., Lubell, J. K., Kim, M. T. and Harris-Warrick, R. M. (1996). Lobster *shal*: comparison with *Drosophila shal* and native potassium currents in identified neurons. *J. Neurosci.* **16**, 1689-1701.

Beck, E. J., Bowlby, M., An, W. F., Rhodes, K. J. and Covarrubias, M. (2002). Remodelling inactivation gating of Kv4 channels by KChIP1, a small-molecular-weight calcium-binding protein. *J. Physiol.* **538**, 691-706.

Bodmer, R. (1993). The gene *tinman* is required for specification of the heart and visceral muscles in *Drosophila*. *Development* **118**, 719-729.

Brahmajothi, M. V., Campbell, D. J., Rasmusson, R. L., Morales, M. J., Trimmer, J. S., Nerbonne, J. M. and Strauss, H. C. (2005). Distinct transient outward potassium current (I_{to}) phenotypes and distribution of fast-inactivating potassium channel alpha subunits in ferret left ventricular myocytes. *J. Gen. Physiol.* **113**, 581-600.

Burgoyne, R. D. and Weiss, J. L. (2001). The neuronal calcium sensor family of Ca^{2+}-binding proteins. *Biochem. J.* **353**, 1-12.

Connor, J. A. and Stevens, C. F. (1971). Prediction of repetitive firing behaviour from voltage clamp data on an isolated neurone soma. *J. Physiol.* **213**, 31-53.

Davidson, B. and Levine, M. (2003). Evolutionary origins of the vertebrate heart: specification of the cardiac lineage in *Ciona intestinalis*. *Proc. Natl. Acad. Sci. USA* **100**, 11469-11473.

Decher, N., Uyguner, O., Scherer, C. R., Karaman, B., Yüksel-Apak, M., Busch, A. E., Steinmeyer, K. and Wollnik, B. (2001). hKChIP2 is a functional modifier of hKv4.3 potassium channels: Cloning and expression of a short hKChIP2 splice variant. *Cardiovasc. Res.* **52**, 255-264.

Decher, N., Barth, A. S., Gonzalez, T., Steinmeyer, K. and Sanguinetti, M. C. (2004). Novel KChIP2 isoforms increase functional diversity of transient outward potassium currents. *J. Physiol.* **557**, 761-772.

Deschênes, I., DiSilvestre, D., Juang, G. J., Wu, R. C., An, W. F. and Tomaselli, G. F. (2002). Regulation of Kv4.3 current by KChIP2 splice variants: a component of native cardiac Ito? *Circulation* **106**, 423-429.

Dixon, J. E., Shi, W., Wang, H. S., McDonald, C., Yu, H., Wymore, R. S., Cohen, I. S. and McKinnon, D. (1996). The role of the Kv4.3 K^+ channel in ventricular muscle: a molecular correlate for the transient outward current. *Circ. Res.* **79**, 659-668.

Dominguez, I., Itoh, K. and Sokol, S. Y. (1995). Role of glycogen synthase kinase 3-beta as a negative regulator of dorsoventral axis formation in *Xenopus* embryos. *Proc. Natl. Acad. Sci. USA* **92**, 8498-8502.

Escriva, H., Manzon, L., Youson, J. and Laudet, V. (2002). Analysis of lamprey and hagfish genes reveals a complex history of gene duplications during early vertebrate evolution. *Mol. Biol. Evol.* **19**, 1440-1450.

Holland, N. D., Venkatesh, T. V., Holland, L. Z., Jacobs, D. K. and Bodmer, R. (2003). *AmphiNk2-tin*, an amphioxus homeobox gene expressed in myocardial progenitors: insights into evolution of the vertebrate heart. *Dev. Biol.* **255**, 128-137.

Holmqvist, M. H., Cao, J., Hernandez-Pineda, R., Jacobson, M. D., Carroll, K. I., Sung, M. A., Betty, M., Ge, P., Gilbride, K. J., Brown, M. E. et al. (2002). Elimination of fast inactivation in Kv4 A-type potassium channels by an auxiliary subunit domain. *Proc. Natl. Acad. Sci. USA* **99**, 1035-1040.

Huelsenbeck, J. P. and Ronquist, F. (2001). MRBAYES: Bayesian inference of phylogenetic trees. *J. Bioinform.* **17**, 754-755.

Hugues, A. L. (1999). Phylogenies of developmentally important proteins do not support the hypothesis of two rounds of genome duplication early in vertebrate history. *J. Mol. Evol.* **48**, 565-576.

Isbrandt, D., Leicher, T., Waldschütz, R., Zhu, X., Luhmann, U., Michel, U., Sauter, K. and Pongs, O. (2000). Gene structures and expression profiles of three human KCND (Kv4) potassium channels mediating A-type currents I_{TO} and I_{SA}. *Genomics* **64**, 144-154.

Jegla, T. and Salkoff, L. (1997). A novel subunit for Shal potassium channels radically alters activation and inactivation. *J. Neurosci.* **17**, 32-44.

Jerng, H. H. and Covarrubias, M. (1997). K^+ channel inactivation mediated by the concerted action of the cytoplasmic N- and C-terminal domains. *Biophys. J.* **72**, 163-174.

Komuro, I. and Izumo, S. (1993). Csx: A murine homeobox-containing gene specifically expressed in the developing heart. *Proc. Natl. Acad. Sci. USA* **90**, 8145-8149.

Kretsinger, R. H. (1987). Calcium coordination and the calmodulin fold: divergent versus convergent evolution. *Cold Spring Harbor Symp. Quant. Biol.* **52**, 499-510.

Kriebel, M. E. (1967). Conduction velocity and intracellular action potentials of the tunicate heart. *J. Gen. Physiol.* **50**, 2097-2107.

Nakajo, K., Katsuyama, Y., Ono, F., Ohtsuka, Y. and Okamura, Y. (2003). Primary structure, functional characterization and developmental expression of the ascidian Kv4-class potassium channel. *Neurosci. Res.* **45**, 59-70.

Nakamura, T. Y., Nandi, S., Pountney, D. J., Artman, M., Rudy, B. and Coetzee, W. A. (2001). Different effects of the Ca^{2+}-binding protein, KChIP1, on two Kv4 subfamily members, Kv4.1 and Kv4.2. *FEBS Lett.* **499**, 205-209.

Notredame, C., Higgins, D. and Heringa, J. (2000). T-Coffee: a novel method for multiple sequence alignments. *J. Mol. Biol.* **302**, 205-217.

Nurmi, A. and Vornanen, M. (2002). Electrophysiological properties of rainbow trout cardiac myocytes in serum-free primary culture. *Am. J. Physiol. Reg. Integr. Comp. Physiol.* **228**, R1200-R1209.

Ohno, S. (1970). *Evolution by Gene Duplication.* Heidelberg: Springer-Verlag.

Page, R. D. (1996). TreeView: an application to display phylogenetic trees on personal computers. *J. Comput. Appl. Biosci.* **12**, 357-358.

Pak, M. D., Baker, K., Covarrubias, M., Butler, A., Ratcliffe, A. and Salkoff, L. (1991). mShal, a subfamily of A-type K^+ channel cloned from mammalian brain. *Proc. Natl. Acad. Sci. USA* **88**, 4386-4390.

Patel, S. P., Campbell, D. L. and Strauss, H. C. (2002). Elucidating KChIP effects on Kv4.3 inactivation and recovery kinetics with a minimal KChIP2 isoform. *J. Physiol.* **545**, 5-11.

Petrecca, K., Miller, D. M. and Shrier, A. (2000). Localization and enhanced current density of the Kv4.2 potassium channel by interaction with the actin-binding protein filamin. *J. Neurosci.* **20**, 8736-8744.

Rivera, J. F., Ahmad, S., Quick, M. W., Liman, E. R. and Arnold, D. B. (2003). An evolutionarily conserved di-leucine motif in Shal K^+ channels mediates dendritic targeting. *Nat. Neurosci.* **6**, 243-250.

Roberds, S. L. and Tamkun, M. M. (1991). Cloning and tissue-specific expression of five voltage-gated potassium channel cDNAs expressed in rat heart. *Proc. Natl. Acad. Sci. USA* **88**, 1798-1802.

Roden, D. M., Balser, J. R., George, A. L., Jr and Anderson, M. E. (2002). Cardiac ion channels. *Annu. Rev. Physiol.* **64**, 431-475.

Romer, A. S. and Parsons, T. S. (1986). *The Vertebrate Body*, 6th edn. Philadelphia: Saunders.

Rosati, B., Pan, Z., Lypen, S., Wang, H. S., Cohen, I., Dixon, J. E. and McKinnon, D. (2001). Regulation of *KChIP2* potassium channel β subunit gene expression underlies the gradient of transient outward current in canine and human ventricle. *J. Physiol.* **533**, 119-125.

Scannevin, R. H., Wang, K., Jow, F., Megules, J., Kopsco, D. C., Edris, W., Carroll, K. C., Lü, Q., Xu, W., Xu, Z. et al. (2003). A fundamental role for KChIPs in determining the molecular properties and trafficking of Kv4.2 potassium channels. *J. Biol. Chem.* **278**, 36445-36454.

Serôdio, P., Kentros, C. and Rudy, B. (1994). Identification of molecular components of A-type channels activating at subthreshold potentials. *J. Neurophysiol.* **72**, 1516-1529.

Serôdio, P., Vega-Saenz de Miera, E. and Rudy, B. (1996). Cloning of a novel component of A-type K^+ channels operating at subthreshold potentials with unique expression in heart and brain. *J. Neurophysiol.* **75**, 2174-2179.

Shibata, R., Misonou, H., Campomanes, C. R., Anderson, A. E., Schrader, L. A., Doliveira, L. C., Carroll, K. I., Sweatt, J. D., Rhodes, K. J. and Trimmer, J. S. (2003). A fundamental role for KChIPs in determining the molecular properties and trafficking of Kv4.2 potassium channels. *J. Biol. Chem.* **278**, 36445-36454.

Sidow, A. (1996). Gen(om)e duplications in the evolution of early vertebrates. *Curr. Opin. Genet. Dev.* **6**, 715-722.

Spreafico, F., Barski, J. J., Farina, C. and Meyer, M. (2001). Mouse DREAM / Calsenilin / KChIP3: Gene structure, coding potential, and expression. *Mol. Cell. Neurosci.* **17**, 1-16.

Spring, J. (1997). Vertebrate evolution by interspecific hybridization-are we polyploid? *FEBS Lett.* **400**, 2-8.

Van Hoorick, D., Raes, A., Keysers, W., Mayeur, E. and Snyders, D. J. (2003). Differential modulation of Kv4 kinetics by KCHIP1 splice variants. *Mol. Cell. Neurosci.* **24**, 357-366.

Wang, S., Patel, S. P., Qu, Y., Hua, P., Strauss, H. C. and Morales, M. J. (2002). Kinetic properties of Kv4.3 and their modulation by KChIP2b. *Biochem. Biophys. Res. Comm.* **295**, 223-229.

Zhang, Y., MacLean, J. N., An, W. F., Lanning, C. C. and Harris-Warrick, R. M. (2003). KChIP1 and frequenin modify *shal*-evoked potassium currents in pyloric neurons in the lobster stomatogastric ganglion. *J. Neurophysiol.* **89**, 1902-1909.